JGR Oceans

RESEARCH ARTICLE
10.1029/2024JC021184

Recent Freshening of the Subpolar North Atlantic Increased the Transport of Lighter Waters of the Irminger Current From 2014 to 2022

Nora Fried[1], Tiago C. Biló[2,3,4], William E. Johns[5], Caroline A. Katsman[6], Kristen E. Fogaren[7], Meg Yoder[7], Hilary I. Palevsky[7], Fiammetta Straneo[8], and M. Femke de Jong[1]

[1]Department of Ocean Systems, NIOZ, Royal Netherlands Institute for Sea Research, Texel, The Netherlands, [2]Cooperative Institute for Marine and Atmospheric Studies, University of Miami, Miami, FL, USA, [3]Atlantic Oceanographic and Meteorological Laboratory, National Oceanic and Atmospheric Administration, Miami, FL, USA, [4]School of Marine Sciences, University of Maine, Orono, ME, USA, [5]Rosenstiel School of Marine, Atmospheric, and Earth Science, University of Miami, Miami, FL, USA, [6]Department of Hydraulic Engineering, Faculty of Civil Engineering and Geosciences, Delft University of Technology, Delft, The Netherlands, [7]Department of Earth and Environmental Sciences, Boston College, Chestnut Hill, MA, USA, [8]Scripps Institution of Oceanography, University of California San Diego, La Jolla, CA, USA

Abstract Starting in 2012, the eastern subpolar North Atlantic experienced the strongest surface freshening in the past 120 years. It is yet unknown whether this salinity anomaly propagated downward into the water column and affected the properties of the boundary currents of the subpolar gyre, which could slow down the overturning. Here, we investigate the imprint of this salinity anomaly on the warm and saline Irminger Current (IC) in the decade thereafter. Using daily mooring data from the IC covering the period 2014–2022 combined with hydrographic sections across the adjacent basins from 1990, the evolving signal of the salinity anomaly over the water column and its imprint on the transport variability is studied. We find that due to the salinity anomaly, the northward freshwater transport of the IC increased by 10 mSv in summer 2016 compared to summer 2015. In 2018, the salinity anomaly covered the water column down to 1,500 m depth. Hydrographic sections across the basin showed that this recent freshening signal spread across the Irminger Sea. Overall, the freshwater transport of the IC increased by a factor of three between 2014–2015 and 2021–2022. The associated density decrease over the upper 1,500 m of the water column resulted in an increase in the northward transport of waters lighter than $\sigma_0 = 27.55$ kg m^{-3} from 1.7 to 4.2 Sv. This change in northward IC transport by density class may impact the characteristics of the overturning in the Northeastern Atlantic, its strength and the density at which it peaks.

Plain Language Summary Starting in 2012, the eastern subpolar North Atlantic experienced the strongest surface freshening in the past 120 years. If these changes in salinity propagate downward in the water column and affect the properties of the boundary currents, this may impact the overturning circulation in the North Atlantic which in turn has a large impact for climate. This paper uses moored observations and hydrographic ship sections to investigate the arrival and evolution of this freshening in the Irminger Current (IC): a current along the western flank of the Reykjanes Ridge in the Irminger Sea that brings warm and saline waters northward. Between 2014 and 2022, those low salinity waters freshened the IC over the upper 1,500 m. In comparison to the observations that exist since the 1990s, by 2022, the IC was fresher than ever and the Irminger Sea was in a similarly fresh state as the previous record of the early 1990s. The net amount of freshwater carried northward by the IC drastically increased over the 8-year time period. This increase in the northward transport of lighter waters could have further implications on overturning in the Irminger Sea.

Key Points:

- Starting in summer 2016, the Irminger Current (IC) freshened over the upper 1,500 m until 2018 and stayed fresh until 2022
- As a result, the northward freshwater transport of the IC increased by a factor of 3 between 2014–2015 and 2021–2022
- The volume transport of waters lighter than $\sigma_0 = 27.55$ kg m^{-3} increased from 1.7 to 4.2 Sv, potentially impacting the overturning

Supporting Information:

Supporting Information may be found in the online version of this article.

Correspondence to:

N. Fried,
nora.fried@nioz.nl

Citation:

Fried, N., Biló, T. C., Johns, W. E., Katsman, C. A., Fogaren, K. E., Yoder, M., et al. (2024). Recent freshening of the subpolar North Atlantic increased the transport of lighter waters of the Irminger current from 2014 to 2022. *Journal of Geophysical Research: Oceans*, *129*, e2024JC021184. https://doi.org/10.1029/2024JC021184

Received 5 APR 2024
Accepted 1 NOV 2024

Author Contributions:

Conceptualization: Nora Fried, Caroline A. Katsman, Fiammetta Straneo, M. Femke de Jong
Data curation: Tiago C. Biló, Kristen E. Fogaren, Meg Yoder, Hilary I. Palevsky, M. Femke de Jong
Formal analysis: Nora Fried, William E. Johns, Kristen E. Fogaren, Meg Yoder, Hilary I. Palevsky
Funding acquisition: Fiammetta Straneo, M. Femke de Jong
Investigation: Nora Fried, William E. Johns, M. Femke de Jong

1. Introduction

The Atlantic Meridional Overturning Circulation (AMOC) is a major component of the climate system. At the surface, the AMOC is responsible for poleward heat transport. At depth, it transports cold and dense water masses formed by deep convection in the Labrador and Irminger Seas (e.g., Lazier, 1973; Lazier et al., 2001; Marshall & Schott, 1999; Pickart et al., 2003; Pickart & Spall, 2007) and Nordic Seas (e.g., Eldevik et al., 2005; Messias et al., 2008; Våge et al., 2015) southward. Previously, AMOC variability was assumed to be primarily linked to

Methodology: Nora Fried, Tiago C. Biló, William E. Johns, Caroline A. Katsman, M. Femke de Jong
Project administration: Fiammetta Straneo, M. Femke de Jong
Software: Nora Fried
Supervision: Caroline A. Katsman, M. Femke de Jong
Writing – original draft: Nora Fried, Tiago C. Biló, Caroline A. Katsman, M. Femke de Jong

variability in Labrador Sea convection (e.g., Thornalley et al., 2018; Yashayaev, 2007; Yeager & Danabasoglu, 2014). However, recent studies highlight the importance of transformation in the Irminger Sea and Iceland Basin to the AMOC variability in the subpolar North Atlantic (Fu et al., 2023; Li et al., 2021).

Due to increasing freshwater input and upper ocean stratification in these high latitude regions, which would act to weaken deep convection, climate models predict an AMOC slowdown. However, the uncertainty on the magnitude and pace of the expected AMOC decrease remains large (Fox-Kemper et al., 2021). Numerous model studies have shown that the release of large amounts of freshwater for an extended period of time can lead to a partial or complete shutdown of the AMOC (e.g., Jackson et al., 2022; Jackson & Wood, 2018; Stouffer et al., 2006). However, intermittent periods of intense freshening of the subpolar North Atlantic on multi-year to decadal time scales have occurred, whose impact on the AMOC remains largely unclear.

From the 1960s to the mid-1990s, the North Atlantic experienced several of these transient freshwater anomalies mostly identified by signals at the surface. Periods of intense surface freshening, so-called "Great Salinity Anomalies" occurred in the 1970s (Dickson et al., 1988), the 1980s (Belkin et al., 1998) and the 1990s (Belkin, 2004).

The freshening from 1967 to 1971 was one of the strongest low-salinity periods observed in the North Atlantic (Dickson et al., 1988; Kim et al., 2021; Lazier, 1980). Earlier studies related the observed shutdown of Labrador Sea convection that occurred during that period to increased stratification due to this low upper ocean salinity (e.g., Gelderloos et al., 2012; Lazier, 1980). Alternatively, the recent modeling results from Kim et al. (2021) suggest the reverse: that the 1970s freshening resulted from decreased Labrador Sea convective activity. The authors showed that this convection suppression was mainly driven by weakened atmospheric forcing. They further argued that it was this reduced convective mixing between the surface and the salty deep ocean that resulted in the observed surface freshening. This shows that it is hard to pinpoint cause and effect between a decrease in salinity and convection.

The freshening event of the 1990s was followed by a period of increasing salinity (Holliday et al., 2008) until a new surface fresh anomaly entered the eastern subpolar gyre in 2012 (Holliday et al., 2020). The decrease in surface salinity is attributed to changes in wind patterns, which in turn resulted in major changes in the ocean circulation (Holliday et al., 2020). Moreover, they showed that this fresh surface signal was strengthened by enhanced precipitation due to unusual atmospheric circulation patterns.

In this paper, we focus on the fate of this recent surface salinity anomaly in the Irminger Sea and analyze how it spread over the water column and changed the local hydrography.

The hydrography of the subpolar North Atlantic has been observed systematically since 1990 with regular repeats of the World Ocean Circulation Experiment AR01E section (WOCE, van Aken et al., 2011) and the Greenland to Portugal OVIDE section (Lherminier et al., 2007; Mercier et al., 2015). Since 2014, AMOC transport in the subpolar gyre has been observed within the basin-wide Overturning in the Subpolar North Atlantic Program that is aligned with the AR01E section (OSNAP, Fu et al., 2023; Li et al., 2021; Lozier et al., 2017, 2019). OSNAP is designed to quantify trans-basin fluxes of volume, heat and freshwater in the subpolar North Atlantic by directly and continuously measuring velocity and property fields. The mooring array spans across the Labrador Sea toward Greenland (OSNAP West) and from Greenland toward the Scottish shelf (OSNAP East, gray dots Figure 1a) across the Irminger Sea, the Iceland Basin and Rockall Trough. The overturning at OSNAP appears to be dominated by its eastern section as shown by the 2-year time series (Fu et al., 2023; Li et al., 2021; Lozier et al., 2019).

In the Irminger Sea, the Irminger Current (IC, Figure 1a) brings relatively warm and saline waters northward along the western flank of the Reykjanes Ridge. It continues cyclonically around the Irminger Sea, flows southward along the east coast of Greenland side by side with the East Greenland Current (EGC) and then turns west into the Labrador Sea at Cape Farewell. On the western flank of the Reykjanes Ridge at the OSNAP East line, the IC is characterized by a two-core structure in the horizontal, with a surface-intensified northward flow in both cores and a southward flow near 1,000 m depth (Chafik et al., 2014; Fried and de Jong, 2022; de Jong et al., 2020; Knutsen et al., 2005; Petit et al., 2019; Sarafanov et al., 2012; Våge et al., 2011, Figure 1b).

As part of OSNAP, a mooring array has been measuring the IC since 2014 (green triangles; Figure 1a). The characteristics of the two IC cores have previously been described: the western core is colder and fresher, the

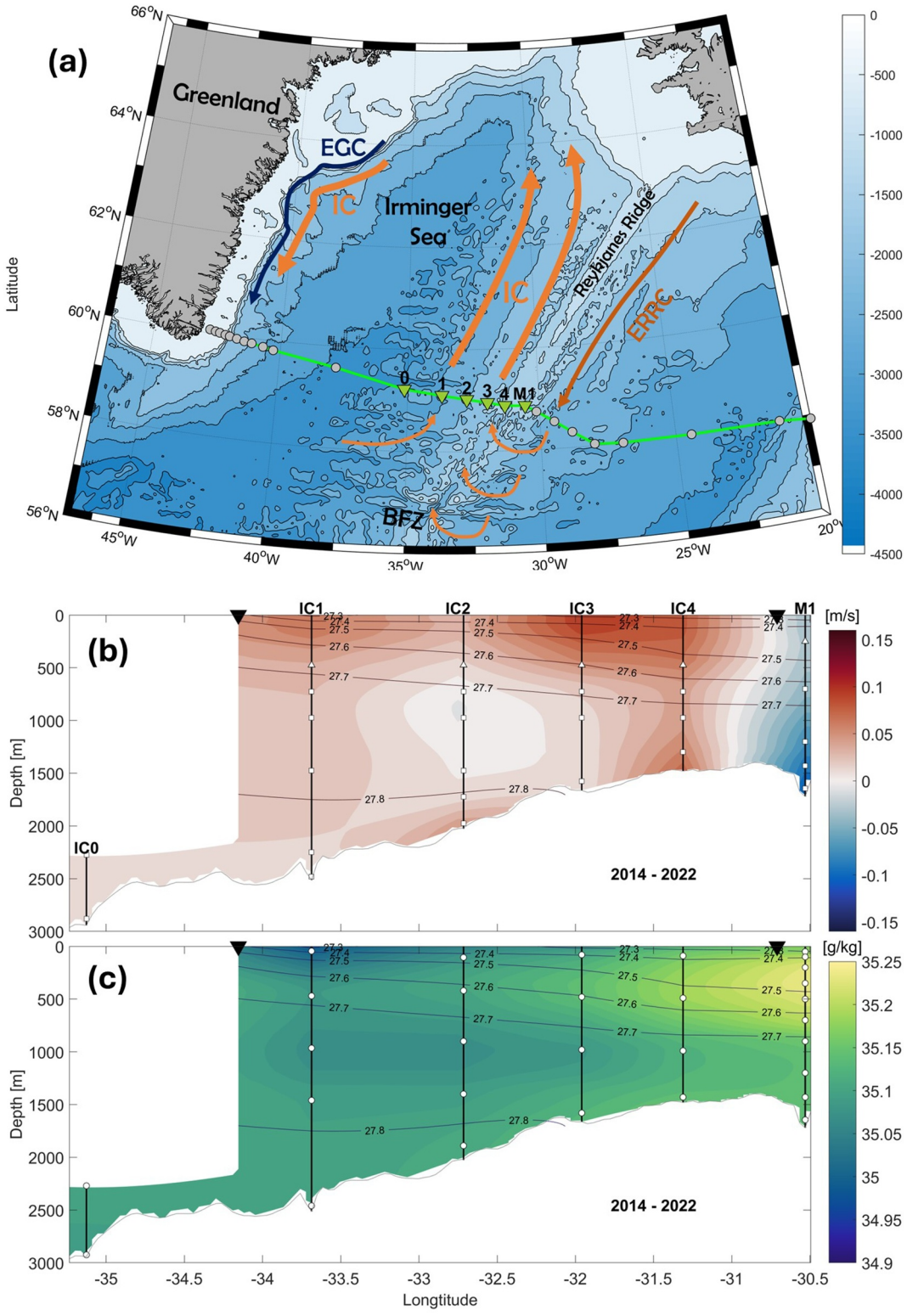

Figure 1.

eastern is core warmer and more saline (Figures 1c, Fried and de Jong, 2022; de Jong et al., 2020; Petit et al., 2019; Våge et al., 2011). At OSNAP East, Fried et al. (2024) identified two main source regions for the two IC cores using a Lagrangian model study: the central Irminger Sea and the Iceland Basin. The western core mostly originates from the central Irminger Sea with a smaller contribution from the Iceland Basin. Reversely, the eastern core has a clear connection to the Iceland Basin and contains a smaller contribution from the central Irminger Sea.

Based on the 2014–2016 time series, de Jong et al. (2020) showed that the mean volume transport in the two IC cores is nearly equal, but that IC variability is dominated by the variability of its western core. The warmer and more saline eastern core is responsible for most of the northward heat and salt transport within the array.

The 2014–2016 time series showed a mean freshwater transport of −22.5 mSv using a reference salinity of 34.92 PSU (de Jong et al., 2020). This negative value of the freshwater transport reflects that the IC is more saline than the reference salinity used to calculate freshwater transports from the OSNAP observations (de Jong et al., 2020) and, in the mean, brings salt northward. Negative freshwater transport can therefore be interpreted as positive northward salt transport.

Since 2016, the IC and the Irminger Sea in general have freshened considerably. The initial arrival of the recent salinity anomaly was described by de Jong et al. (2020). They showed that the anomaly arrived in summer 2016 in the near surface layer of the easternmost IC mooring. The arrival and impact of the surface salinity anomaly in the central Irminger Sea was investigated by Biló et al. (2022). They emphasize that it resulted in fresher convective waters in 2017–2018 compared to previous winters and that it contributed to suppressing the convection in the following winters. Here, we will show that, since then, the anomaly has transitioned from a near surface anomaly to a general freshening of upper 1,500 m of the water column with implications for the northward volume transport by density class that the IC carries.

This paper is organized as follows: Section 2 introduces the mooring data and hydrographic sections as well as the data postprocessing procedure. Section 3 discusses the downward propagation and spread of the salinity anomaly at the mooring array throughout the 8-year record. Section 4 puts the recent freshening in the IC into perspective of changes in the whole Irminger Sea and Iceland Basin and compares it to salinity changes in the Irminger Sea over a 30-year time period. Section 5 focusses on the impacts of the freshening on the density structure and transport variability of the IC. The strong decrease in salinity at the IC array will be discussed with respect to literature in Section 6.

2. Data and Methods

2.1. The Irminger Current Mooring Array

In July 2014, the Royal Netherlands Institute for Sea Research (NIOZ) first deployed five moorings on the western flank of the Reykjanes Ridge to directly measure the volume, heat and freshwater transports of the IC. The moorings belong to the OSNAP sub-section OSNAP East. Here, we analyze the full 8-year time series that is available up to July 2022.

The NIOZ mooring array consists of four long (IC1-4) and one short mooring (IC0) within the two-core structure of the IC (Figures 1a and 1b). To determine the boundary between the southward flow of the East Reykjanes Ridge Current (ERRC) and the northward flow of the IC, we include the tall mooring M1 (maintained by the University of Miami) on the eastern side of the Reykjanes Ridge in our analysis. The four long moorings reach from the bottom up to ∼60 m below the sea surface and measure velocity, temperature, and salinity. The moorings are equipped with upward looking ADCPs (Acoustic Doppler Current Profiler, RDI 75 kHz Long Ranger) and single point current meters (CM, Aanderaa RCM11 or Nortek Aquadopps) to measure the velocity field. We use Sea-Bird Electronics SBE37 (MicroCATs) and Sea-Bird Electronics SBE56 (thermistors) to measure temperature

Figure 1. Schematic overview of the circulation in the Irminger Sea and hydrography of the Irminger Current. (a) Schematic main currents in the Irminger Sea: Irminger Current (IC), East Reykjanes Ridge Current (ERRC) and East Greenland Current (EGC) and bathymetric features: Bight Fracture Zone (BFZ) and Reykjanes Ridge. Gray dots: OSNAP East moorings, green triangles: IC array moorings 0–4 and M1; Green line represents the hydrography line, (b) velocity (shading, m s^{-1}) and density (contours, kg m^{-3}) across IC section averaged over the years 2014–2022, (c) as (b) but for salinity (g kg^{-1}). In (b, c), black vertical lines mark the mooring locations; white icons mark the depth of various types of instruments (triangles, ADCPs; squares, current meters; circles, MicroCATs); black triangles mark the IC boundaries used for transport calculations; the gray line delineates the bottom topography.

and salinity. The short mooring IC0 only covers the lower 700 m of the water column and is equipped with MicroCATs and CMs only. The M1 mooring has an upward-looking ADCP, Nortek Aquadopp current meters and MicroCATs (see Koman et al., 2020 for additional information on M1). Sampling intervals are 1 hr for the ADCPs, 30 min for the CM, 15 min for the MicroCATs, and 5 min for the thermistors.

2.2. Mooring Data Processing

All data processing consistently involved the following steps. First, the data were low-pass filtered with a 41-hr Butterworth filter to remove tides and inertial motion and subsampled on a daily grid. Next, all profiles were vertically interpolated with the MATLAB "pchip" function and horizontally interpolated linearly on a grid with bottom-following contours. The IC flows in a north–east direction along the ridge with an angle to the mooring array. To be able to compute transports across the array, we then rotated the horizontal velocity components clockwise by 10°. The resulting velocities are now aligned with the orientation of the array line and approximately with the main flow direction.

After filling the data gaps, we obtained daily fields of along- and across-stream velocity, potential temperature and practical salinity from 2014 to 2022 (see Supporting Information S1 for details). Finally, we converted the observed potential temperature and practical salinity to conservative temperature and absolute salinity using TEOS-10 (McDougall & Barker, 2011). Yearly means discussed in the text are computed from summer to summer (1st of August–31st of July). For a more detailed description of the data processing the reader is referred to de Jong et al. (2020) and Fried and de Jong (2022).

2.3. Volume, Heat, and Freshwater Transport

From the mooring data we calculated volume, heat and freshwater transports following de Jong et al. (2020) and Fried and de Jong (2022). Volume transport estimates were derived from the daily fields. The total volume transport V is defined as

$$\mathrm{V}(t) = \int_{\mathrm{X_w}}^{\mathrm{X_e}} \int_{\mathrm{Z_{max}}}^{0} v(x,z,t)\, dz dx \left[\text{ in Sv} = 10^6\ \mathrm{m^3 s^{-1}}\right], \tag{1}$$

where v is across-array velocity, X_w (34.1°W) and $\mathrm{X_e}$ (30.7°W) are the western and eastern boundaries, respectively (indicated by black triangles in Figures 1b and 1c, following Våge et al. (2011)), and $z = 0$ and $Z_{\max}$ are the surface and bottom boundaries.

We calculated the heat transport H with respect to a reference temperature $T_{\mathrm{ref}} = 0$°C using:

$$\mathrm{H}(t) = \int_{\mathrm{X_w}}^{\mathrm{X_e}} \int_{\mathrm{Z_{max}}}^{0} \rho(x,z,t)\, c_p\,(x,z,t)\, v(x,z,t)\, (T(x,z,t) - T_{\mathrm{ref}})\, dz dx \left[\text{in PW} = 10^{15}\ \mathrm{W}\right], \tag{2}$$

where ρ is density and c_p is the specific heat capacity. Both were calculated per time step from the gridded fields using TEOS-10 toolbox (McDougall & Barker, 2011).

The freshwater transport F was calculated using:

$$\mathrm{F}(t) = \int_{X_w}^{X_e} \int_{Z_{\max}}^{0} v(x,z,t) \left(1 - \frac{S(x,z,t)}{S_{\mathrm{ref}}}\right) dz dx \text{ [in mSv]} \tag{3}$$

where S is the practical salinity [PSU] and $S_{\mathrm{ref}} = 34.92$ PSU is the reference salinity (compare de Jong et al., 2020; Lozier et al., 2019). As the IC has a higher salinity than this reference value, adopting this definition yields a negative freshwater transport.

To investigate the transport changes in different parts of the water column, we also computed these transports V, H, and F for three different density classes. We used the potential density σ_0 (hereafter interchangeably referred to as density for simplicity) of maximum overturning in OSNAP 27.55 kg $\mathrm{m^{-3}}$ as a separation between upper and lower AMOC density classes (Fu et al., 2023; Li et al., 2021). Additionally, we defined waters denser than

27.8 kg m^{-3} as overflow waters. Hence, we considered three layers: from the surface to the 27.55 kg m^{-3} isopycnal (Layer 1), between the 27.55 and 27.8 kg m^{-3} isopycnals (Layer 2) and below the 27.8 kg m^{-3} isopycnal (Layer 3).

2.4. Hydrographic Sections at OSNAP East

To quantify the hydrographic changes the Irminger Sea underwent within the last 30 years we used hydrographic sections across the Irminger Sea and the Iceland Basin along the WOCE AR01E repeat section (van Aken et al., 2011) and the Greenland to Portugal OVIDE section (Lherminier et al., 2007; Mercier et al., 2015). The AR01E section aligns with the OSNAP East line and therefore allows us to link changes at the IC mooring array to basin-wide changes over a longer time period. This section has been observed with ships since 1990, nearly every year, mostly in summer. During the 2022 occupation of the OSNAP East section, dissolved oxygen was measured using a SBE43 sensor and calibrated using discrete water samples measured for oxygen using shipboard Winkler titrations.

All section data were vertically interpolated to a regular 1 m depth grid. To account for the unequal number of CTD stations occupied each year, we created a grid along the OSNAP East section with 0.1° resolution in the horizontal, inserted the data to the nearest grid point, and interpolated horizontally. From the 6 summer occupations of the section between 2014 and 2022 we computed a mean (referred to as "OSNAP mean").

To put recent salinity changes into a long-term perspective we specifically focus on two sections both taken in September: 1992 and 2005. Those 2 years best mark the extreme salinity variations in the Irminger Sea in the past 30 years: in 1992 the Irminger Sea was freshest and in 2005 it was most saline. To compare changes in the IC's salinity between different years, we calculated mean vertical profiles of salinity between 34.1° and 30.7°W (black triangles Figures 1b and 1c) from these hydrographic sections.

3. Salinity Changes in the Irminger Current

To assess the hydrographic changes within the IC, we first investigate the spread of the near-surface salinity anomaly over the whole water column across the IC mooring array between 2014 and 2022.

The recent salinity anomaly described by Holliday et al. (2020) circulated in the eastern subpolar gyre between 2012 and 2016. The arrival and subsequent deepening of this freshening signal at the IC moorings is highlighted by plotting the evolution of the salinity anomaly with respect to the 8-year mean. Here, we show the salinity anomalies from IC2 (Figure 2a), near the western edge of the eastern IC core (Figures 1b and 1c), and from IC4 (Figure 2b), which is located in the most saline waters of the IC near the top of the Reykjanes Ridge. To investigate the arrival of the salinity anomaly in the Irminger Sea, we show M1 located upstream on the eastern side of the Reykjanes Ridge (Figure 2c).

The first sign of the negative salinity anomaly at the moorings can be seen around summer 2016 in the upper 300 m. At IC4, the anomaly gradually extends deeper into the water column through 2017–2018 and is seen at depths down to 1,500 m by summer 2018 (Figure 2b). At IC4, the anomaly is 0.05 g kg^{-1} stronger than at IC2. At IC2, the anomaly covers the upper 1,500 m in winter 2017/2018. IC2 shows more short-term variability overlaying the interannual signal.

There is an overall decrease in density of the upper 500 m associated with the freshening of the water column at all moorings (contour lines in Figure 2). As a result, the isopycnal commonly used to describe the maximum subpolar overturning (i.e., $\sigma_0 = 27.55$ kg m^{-3}) deepens. While this isopycnal was outcropping during winter in 2014 and 2015, it stays well below 300 m after summer 2018 until the end of the timeseries. Additionally, the deep isopycnal commonly used to describe the overflow waters (i.e., $\sigma_0 = 27.8$ kg m^{-3}) retreats westward, disappearing from the IC4 records in 2018. The evolution and timing on the eastern side of the ridge at M1 is very similar to IC4, suggesting the connection of the two currents. The freshening at depth at IC4 and M1 is likely related to entrainment of fresh intermediate waters, related to the salinity anomaly, into the overflow waters in the Iceland Basin (Devana et al., 2021).

To get a better sense of the temporal and spatial evolution of the salinity over the whole IC, Figure 3 displays annual mean salinity anomalies with respect to the 8-year mean salinity that was shown in Figure 1c. The year 2014–2015 appears to be by far the most saline year in the 8-year record (Figure 3a). Especially the upper 500 m

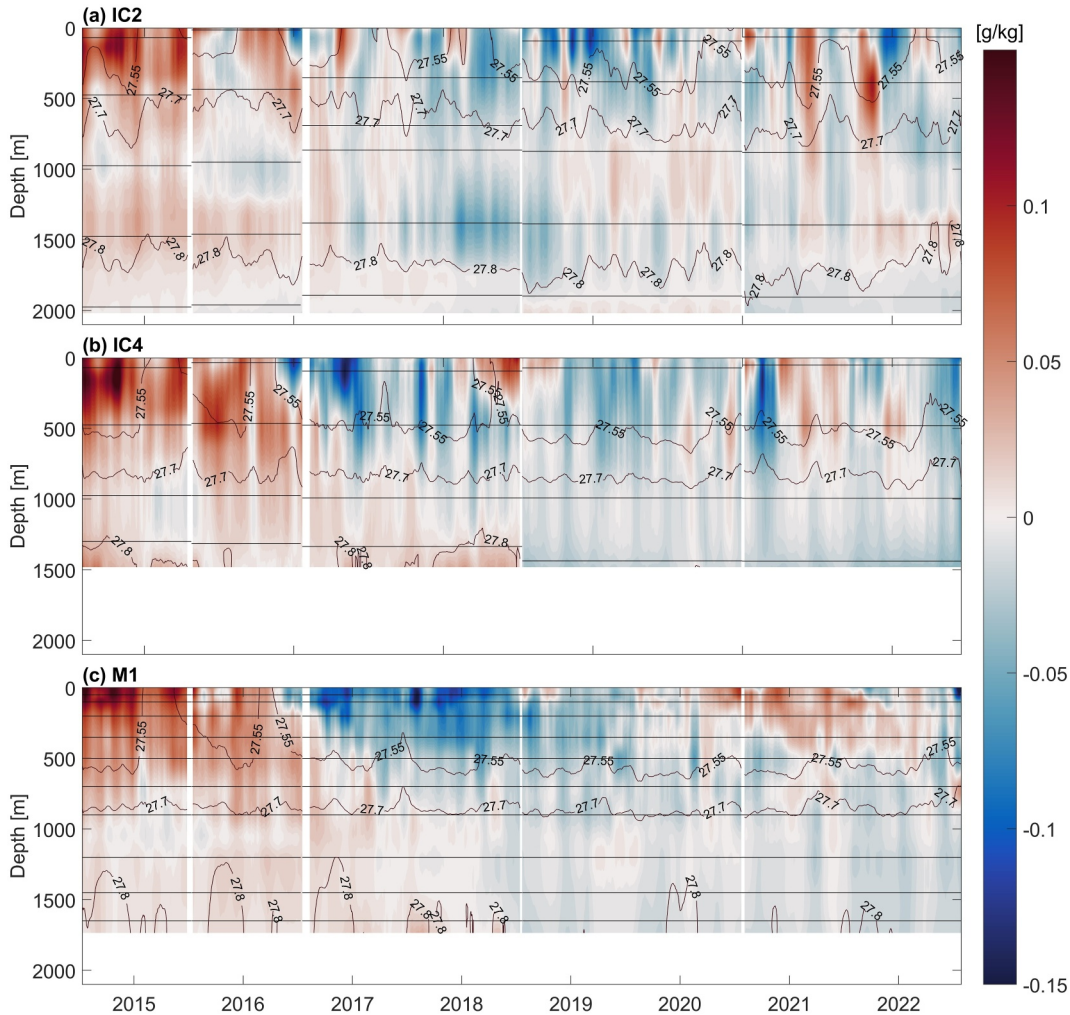

Figure 2. Salinity evolution at IC2, IC4, and M1 Daily salinity anomalies from IC2 (a), IC4 (b) and M1 (c) mooring (shading) overlaid with potential density (contours). The anomalies are computed by removing the 2014–2022 mean salinity and seasonal cycle at each location and depth. Horizontal black lines mark instrument depths for respective deployment periods.

show a strong positive salinity anomaly across the whole array compared to the 8-year mean (+0.09 g kg^{-1}). This is weaker but still positive in 2015–2016 (Figure 3b). In 2016–2017, a negative salinity anomaly becomes visible in the upper 500 m, most pronounced between IC4 and M1 (−0.06 g kg^{-1}, Figure 3c). In 2017–2018, the anomaly spreads to larger depths in the middle of the array. A slight positive anomaly remains at IC1 below 1,000 m and at IC4 (0.01 g kg^{-1}, Figure 3d). By 2018–2019, the negative salinity anomaly covers the whole array, but its amplitude is weaker (−0.01 to −0.05 g kg^{-1}, Figure 3e) as the signal is gradually diluted. Between 2019 and 2021 (Figures 3f and 3g), the anomaly weakens even further. Some saline waters reappear resulting in slightly positive anomalies in the eastern part of the array. In 2021–2022, fresher waters appear in the upper 300 m again, reflected as a negative salinity anomaly (about −0.03 g kg^{-1}), particularly at the surface at IC1.

The decrease in salinity across the IC array (Figure 2) will affect the density structure (see evolution of isopycnals Figure 2). To quantify the effect of these salinity variations on density, we computed the density anomaly by linearizing the equation of state (see Supporting Information S1). As a result, we are able to isolate the salinity and temperature contributions to the density anomalies (Figure 4). In addition, we show the sum of the contribution of temperature and salinity (total, black line) and the density anomaly as observed (gray line). The total and observed density anomaly only show minor differences and exhibit the same overall variability ($r = 0.97$). Both show a negative trend of similar strength (−0.0046 and −0.0045 kg m^{-3} per year, respectively). As the linearization only fails for very short periods of time (e.g., autumn 2015), it is a good approximation. The temperature is strongly

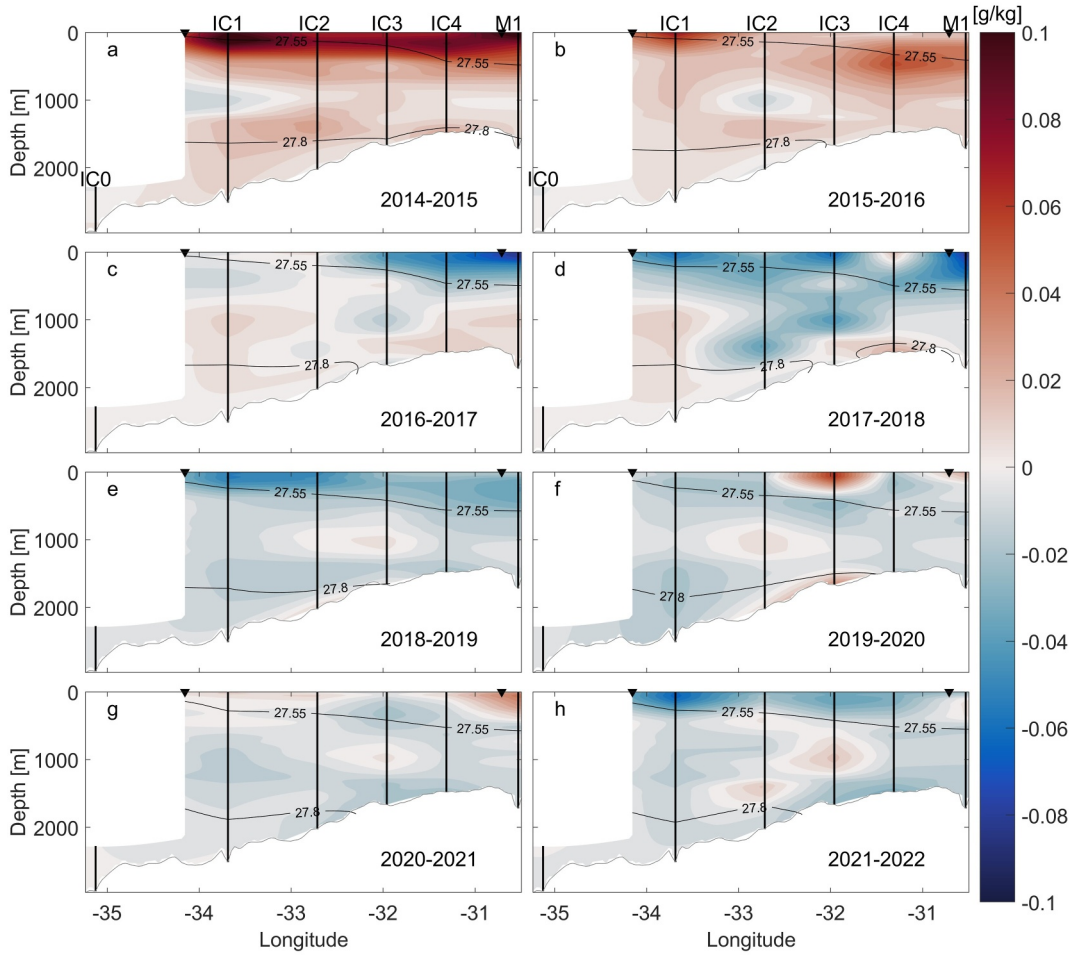

Figure 3. Annual mean salinity anomalies for IC array from 2014 to 2022 Salinity anomalies from summer to summer for the IC referenced to the mean salinity over 2014–2022 (color) with yearly mean isopycnals. Black triangles at the surface mark the IC boundaries. Black vertical lines mark the mooring locations.

correlated to the total density anomaly ($r = 0.84$) but is mostly responsible for the annual to seasonal variability in density (green line). It only shows a very weak negative trend (-0.00087 kg m^{-3} per year). This negative trend in the density anomaly is related to the decrease in salinity due to freshwater anomaly (orange line, 0.0037 kg m^{-3} per year). Therefore, the salinity changes are responsible for the decrease in density on interannual timescales, which dominates over the density changes related to temperature.

4. Salinity Changes Along OSNAP East

In the following, we investigate the spatial extent of the freshening signal. Since we have a long observational record of salinity from hydrographic sections, we can put the changes in the IC (Section 3) into the perspective of changes in the Irminger Sea and Iceland Basin.

In Figure 5, we compare the salinity changes found at the IC array to changes along the whole AR01E section from single summer snap-shots in the form of hydrographic sections. We focus on the most recent 2022 section at OSNAP East, which exhibited the most widespread salinity anomaly at the IC array, and contrast that with the section from 2014, which was most saline (Figures 3a and 3h). In addition, we compare these sections to those from the years 2005 to 1992, which both mark extreme years in salinity within the past 30 years of observations along the AR01E section. Figure 5a shows a mean TS-diagram of the averaged water mass properties over the upper 1,000 m and over the entire section from all 25 CTD sections between 1990 and 2022. It illustrates that the years 1992 and 2005 contrast the fresh state of the 1990s with the very warm and saline mid-2000's. When only

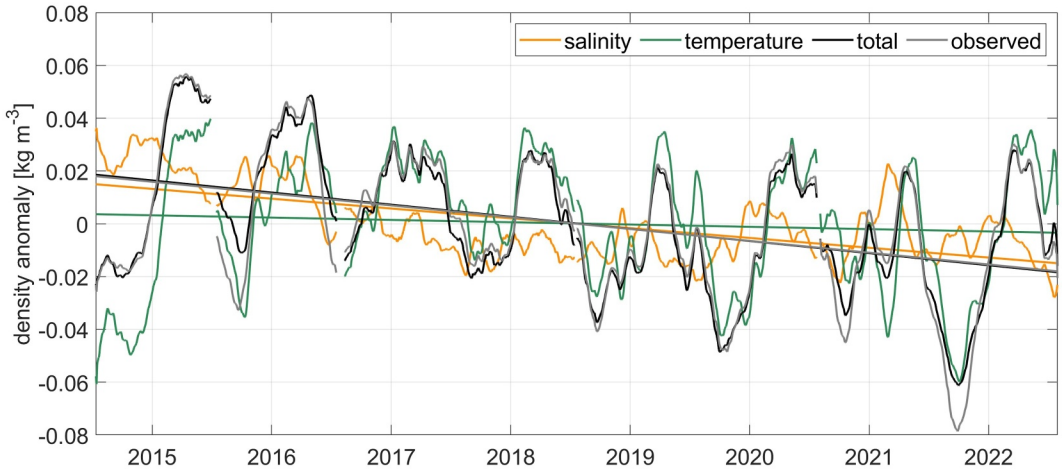

Figure 4. Contribution of temperature and salinity to the density anomaly time series of the density anomaly over the entire IC related to salinity (orange), temperature (green), the sum of both (total, black), and the observed (gray) in kg m^{-3}. The density anomalies are computed by linearizing the equation of state between the IC boundaries (black triangles Figures 1b and 1c) relative to the 8-year mean over the whole water column (see Supporting Information S1). The daily time series is smoothed by 30 days, and the linear trends (solid lines) are computed from these smoothed time series. All linear trends are negative: salinity (−0.0037 kg m^{-3} per year), temperature (−0.00087 kg m^{-3} per year), sum (−0.0046 kg m^{-3} per year), observed (−0.0045 kg m^{-3} per year).

the IC is considered (Figures 5b), 1992 still represents the freshest state recorded before the year 2022. In the year 2005, the IC does not display a particularly high salinity.

The OSNAP mean over 2014–2022 (Figure 5c) exhibits higher salinities in the Iceland Basin compared to the Irminger Sea, where most saline waters can be found over the top of the Reykjanes Ridge. In the central Irminger Sea, we find low salinity waters typically known as Labrador Sea Water. Those waters are either formed in the Labrador Sea and exported to the Irminger Sea or formed by local convection in the Irminger Sea itself (de Jong & de Steur, 2016; de Jong et al., 2012, 2018; Piron et al., 2016; Pickart et al., 2003). The $\sigma_0 = 27.55$ kg m^3 -isopycnal exhibits a strong slope in the vicinity of the IC, marking its strongest horizontal pressure gradients and velocities.

In summer 2022, most of the section is characterized by a negative salinity anomaly (−0.01 g kg^{-1}, Figure 5d). This decrease in salinity is strongest over the Reykjanes Ridge (−0.1 g kg^{-1}), where typically the most saline waters in this section are found (Figure 5c). While at that time waters below 300 m in the Iceland Basin are more saline than average, the Irminger Sea is slightly fresher. The freshening in 2022 is especially obvious when comparing it to the conditions in the summer of 2014 (Figure 5e). At that time the positive salinity anomaly is not limited to the IC but extends across the whole section in the upper 700 m with a positive salinity anomaly (0.1 g kg^{-1}). Below, in the layers associated with Labrador Sea Water, the Iceland Basin is slightly fresher than average (−0.002 g kg^{-1}). The Iceland Basin also displays a negative salinity anomaly below 700 m (−0.05 g kg^{-1}).

This shows that recent changes observed at the IC mooring array do extend into the Irminger Sea. But are these changes associated with the recent salinity anomaly exceptional? Long-term hydrographic changes in the central Irminger Sea are described by van Aken et al. (2011) and de Jong et al. (2023). They identified the early 1990s as the freshest period in the record since 1950. At the IC, the 2005-section exhibits a thin fresh summer layer at the surface that results in a slightly fresher TS-mean for the IC compared to the mean of the entire section (Figures 5a, 5b, and 5f). The hydrographic section of 2005 reveals a positive salinity anomaly the upper 1,000 m, strongest in the Iceland Basin (Figure 5f). Note that the Iceland Scotland Overflow Water (ISOW, $\sigma_0 \geq 27.8$ kg m^{-3}) layer is also saltier than average, probably because of the rapid entrainment of saline Atlantic waters in the ISOW plume (e.g., Chafik & Holliday, 2022; Devana et al., 2021). In contrast, in the Irminger Sea, the waters below the 27.8 kg m^{-3} -isopycnals are fresher. In 1992, all water masses over the entire section are fresher than average (Figure 5g), and the signal is stronger than in 2022. Especially the Iceland Basin is very fresh compared to the OSNAP mean. Holliday et al. (2020) showed that the recent salinity anomaly peaked in 2016–2017 in the Iceland

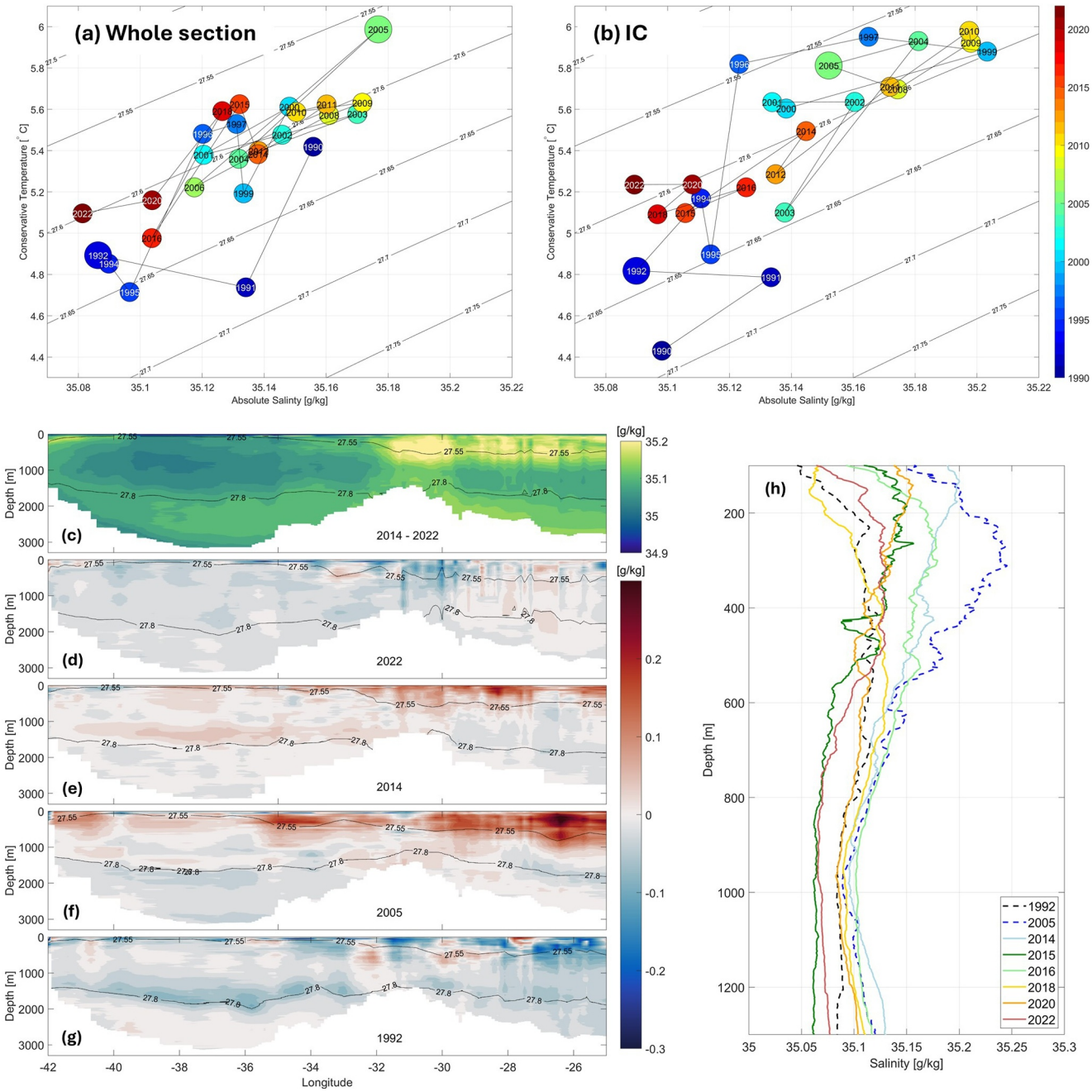

Figure 5. Salinity evolution at OSNAP East between 1990 and 2020. (a, b) Mean TS-properties of the waters in the upper 1,000 m from hydrographic sections over the period 1992 to 2022, (a) for the entire section and (b) IC region. Colors indicate the years. (c) Mean salinity from hydrographic sections for the OSNAP period 2014–2022 (shading) with isopycnals (contours); (d–g) salinity anomaly (shading) with respect to the 8-year mean in (c) with mean isopycnals for that year (contours) for (d) 2022, (e) 2014, (f) 2005, and (g) 1992. (h) IC salinity profiles averaged between 34.1°W and 30.7°W for all hydrographic sections for the OSNAP time period 2014–2022 (solid, colored lines) and for 1992 and 2005 (dashed lines).

Basin. By 2022, the anomaly in the Iceland Basin has diluted and weakened and therefore appears less strong. So, the recent freshening along the OSNAP East section freshened waters to a comparable state as in the 1990s.

To further investigate the salinity evolution and stratification of the IC, Figure 5h shows vertical salinity profiles. The 1992 profile (black dashed line in Figure 5h) shows very little stratification in salinity, the result of deep convective mixing within the boundary current in preceding winters. Deep convection ceases around 1995, and a period of predominantly weak winters lasts until 2007 (de Jong et al., 2023). During the late 1990s and early

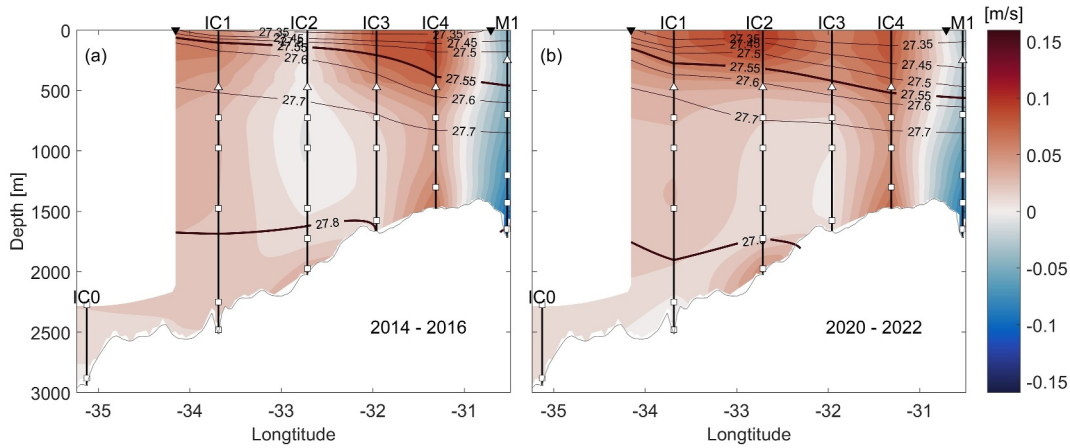

Figure 6. Across-section velocities at IC array (a, b) 2-year mean velocity across array (shading) and isopycnals (contours) for (a) 2014–2016 and (b) 2020–2022. Black triangles at the surface mark the IC boundaries. Moorings are marked by black vertical lines (IC0-IC4, M1). Blue (red) shading mark southward (northward) velocities. Current meters and ADCPs are marked by white boxes/triangles, respectively. Gray line marks the bottom topography.

2000s, the basin slowly restratifies with warmer, more saline water. The 2005 profile (blue dashed line in Figure 5h) shows a salinity minimum at 1,000 m, a remnant of convective waters, with strongly increasing salinity upwards to around 300 m. These upper waters are the warm, saline waters with an IC origin. A thin fresher layer is found at the top, typical for summer stratification (Sterl & de Jong, 2022). Below 100 m, the IC is most saline compared to the OSNAP years and 1992. Since 2005, there has been intermittent convection until the winter of 2014/2015, but not strong enough to halt the seasonal restratification of the basin (de Jong et al., 2023). Exceptionally strong convection events occurred in the winters of 2014–2015 and 2015–2016 (de Jong & de Steur, 2016; de Jong et al., 2018). The 2014 (summer) profile shows the salinity of the water column before that event. It shows that most of the water column had become more saline than in 2005, except for the 200–500 m layer. In contrast, the 2015 profile is much fresher except for the uppermost layer. The 2016 profile shows high salinity throughout the water column except for the upper 200 m. The freshening near the surface in August 2016 marks the onset of the salinity anomaly. The 2018 profile in turn is much fresher in the upper 600 m than in 2016. Between 150 and 250 m the 2018 profile is even fresher than the profile from 1992. The 2020 profile shows that salinity in the upper 300 m increased again. In 2022, the waters above 250 m freshens. At depth, below 500 m, the downward mixing of the salinity anomaly make the IC even fresher than in 1992.

At the IC array, the recent freshening at the surface is comparable to 1992. The waters below 500 m are even about 0.03 g kg^{-1} fresher in 2022 than in 1992. The freshening along OSNAP East is comparable to the fresh state in the 1990s with the anomaly peaking in 2016–2017 in the Iceland Basin and in 2018–2019 in the Irminger Sea.

5. Changes in the Irminger Current's Velocity Structure and Transports

To assess the potential of the recent salinity anomaly to impact the AMOC's upper limb, we investigate the implications of the observed salinity and density changes on the velocity structure of the IC and its volume, heat and freshwater transports.

As shown in Figure 4, the strong interannual changes in salinity are not compensated by strong changes in temperature. Therefore, resulting changes in the density structure can primarily be attributed to the presence of the salinity anomaly. The changes in salinity in turn could have affected the velocity structure of the IC by changing the slope of the isopycnals. A comparison of the IC velocity structure before the arrival of the salinity anomaly and at the time that it is at its freshest (Figure 6) indeed shows clear differences. The 2014–2016 mean velocity displays a clear two-core structure separated by a very weak southward flow at intermediate depth (Figure 6a). In 2020–2022, the western core moves closer to the eastern core and the southward flow around IC2 at 1,000 m depth disappears (Figure 6b), while the region below 1,500 m at IC3 is still characterized by weak velocities. For the western core, the maximum velocity in the upper layer increases compared to 2014–2016. This results in an increase in vertical shear, consistent with a thermal wind response to an increase in the density gradient along the

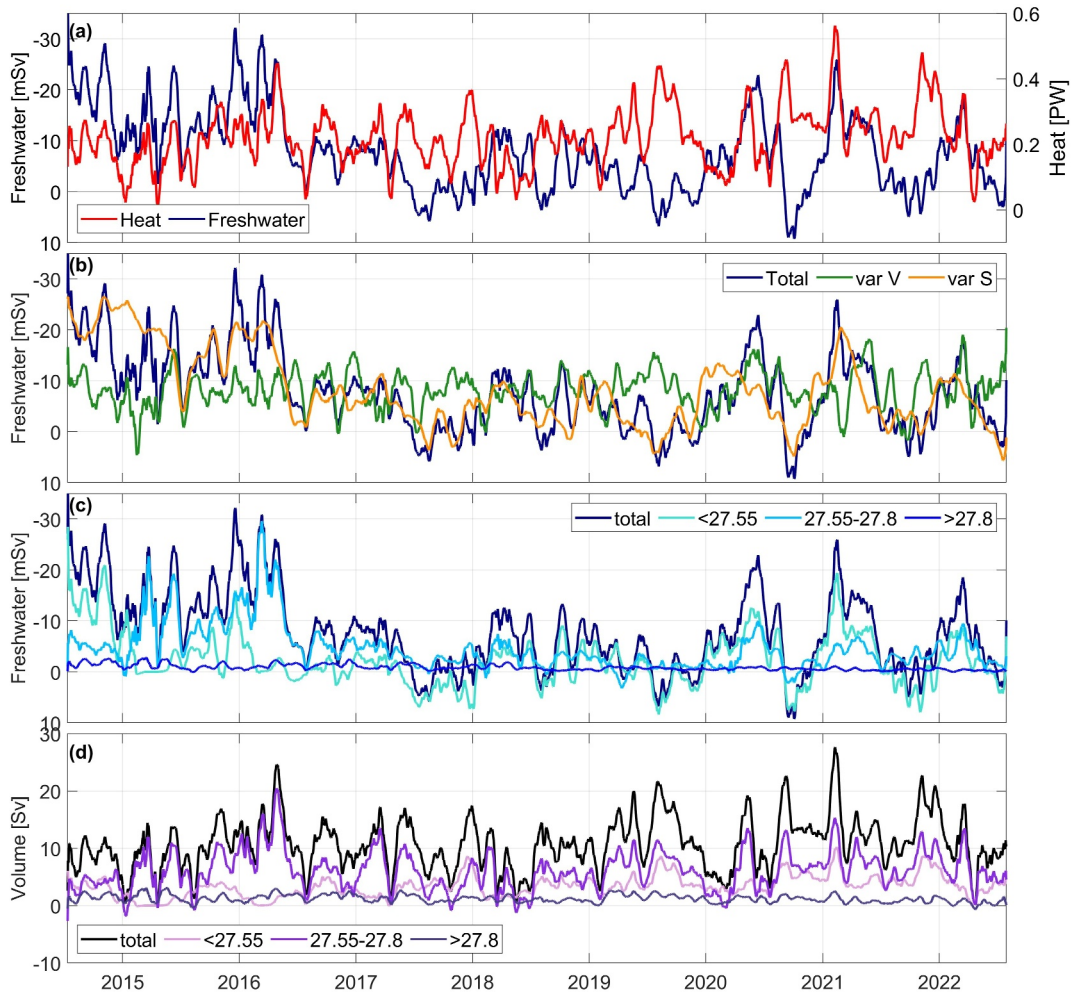

Figure 7. Transports of the Irminger Current Daily transport time series from IC mooring data smoothed by 30 days from 2014 to 2022 for (a) freshwater transport (blue, mSv, left axis) and heat transport (red, PW, right axis); note that the axis for freshwater transport is reversed to represent northward salt transport; (b) total freshwater transport (total, blue), split by the contributions from mean salinity and a variable velocity field (varV, green) and from the mean velocity and a variable salinity field (varS, orange); (c) freshwater transport by density classes: total (dark blue, Sv), lighter than $\sigma_0 = 27.55$ kg m^{-3} isopycnal (cyan), between 27.55 and 27.8 kg m^{-3} (light blue) and denser than 27.8 kg m^{-3} (blue); (d) volume transport total (black, Sv), lighter than $\sigma_0 = 27.55$ kg m^{-3}- isopycnal (pink), between 27.55 and 27.8 kg m^{-3} (purple) and denser than $\sigma_0 = 27.8$ kg m^{-3} (dark purple).

section. In addition to such thermal wind response, the changes in velocity structure (Figure 6) may also be partly attributable to changing atmospheric conditions. The strong positive phase of the North Atlantic Oscillation (NAO) from 2014 to 2020 (Yashayaev, 2024) likely built up the strength of the subpolar gyre and with that might have resulted in a stronger IC.

Lastly, we analyze the imprints of the salinity anomaly on the freshwater, heat, and volume transports of the IC within the longitude range of the mooring array (Figure 7). As explained in Section 2.3, for the IC, the northward freshwater transport (Equation 3) is negative because the salinity of the IC is higher than the chosen reference salinity. A negative IC freshwater transport therefore represents a northward transport of salt. To visualize the decrease or increase in salinity of the saline IC in a more intuitive way, we reverse the axis for freshwater transport (Figure 7). A minimum (maximum) in freshwater transport represents a decrease (increase) in northward salt transport. The mean freshwater transport over the 8-year time series is -7.8 ± 12.9 mSv.

The freshwater transport drastically changes from -15.8 mSv in 2015–2016 to -5.8 mSv in 2016–2017 (blue line in Figures 7a, Table 1) with the arrival of the salinity anomaly at the IC array. Those numbers indicate the

Table 1
Yearly Mean Values for Freshwater, Heat and Volume Transport From Daily Time Series Upper Row: Total Freshwater Transport With Standard Deviation (mSv) Together With Freshwater Transport Split Into Density Layers

	14/15	15/16	16/17	17/18	18/19	19/20	20/21	21/22
Freshwater (mSv)	**−15.2** ± 17.5	**−15.8** ± 14.6	**−5.8** ± 8.3	**−3.5** ± 9.9	**−3.8** ± 8.3	**−5.8** ± 11.1	**−7.3** ± 12.2	**−4.1** ± 10.6
F < 27.55 kg m^3	−6.4 ± 9.4	−3.0 ± 6.5	−0.1 ± 5.1	0.3 ± 6.6	−1.5 ± 6.4	−2.5 ± 7.6	−4.1 ± 9.2	−0.2 ± 7.9
27.55 < F < 27.8	−7.3 ± 13.9	−11.7 ± 12.2	−4.4 ± 4.6	−3.0 ± 5.3	−1.7 ± 3.3	−2.7 ± 4.9	−2.6 ± 3.9	−3.5 ± 4.1
F > 27.8 kg m^3	−1.5 ± 1.5	−1.1 ± 1.0	−1.3 ± 1.1	−0.9 ± 0.9	−0.6 ± 0.5	−0.6 ± 0.6	−0.5 ± 0.5	−0.4 ± 0.5
Heat (PW)	**0.17** ± 0.17	**0.23** ± 0.18	**0.21** ± 0.15	**0.17** ± 0.16	**0.22** ± 0.14	**0.22** ± 0.17	**0.29** ± 0.15	**0.25** ± 0.17
Volume V (Sv)	**8.3** ± 8.5	**11.7** ± 9.4	**10.8** ± 7.8	**7.8** ± 8.2	**11.2** ± 7.2	**10.4** ± 8.6	**13.9** ± 7.7	**11.7** ± 8.8
V < 27.55 kg m^3	1.7 ± 2.3 (21%)	2.0 ± 1.9 (17%)	2.8 ± 2.3 (25%)	3.3 ± 2.7 (42%)	3.7 ± 2.4 (33%)	3.8 ± 2.9 (36%)	5.1 ± 2.8 (37%)	4.2 ± 3.1 (36%)
27.55 < V < 27.8	5.0 ± 7.4 (60%)	8.3 ± 8.3 (71%)	6.5 ± 5.9 (60%)	3.5 ± 6.2 (45%)	6.2 ± 4.8 (55%)	5.5 ± 6.1 (53%)	7.7 ± 5.1 (55%)	6.7 ± 6.1 (58%)
V > 27.8 kg m^3	1.6 ± 1.6 (19%)	1.4 ± 1.3 (12%)	1.5 ± 1.4 (15%)	1.0 ± 1.1 (13%)	1.3 ± 1.3 (12%)	1.2 ± 1.2 (11%)	1.1 ± 1.0 (8%)	0.7 ± 1.2 (6%)

Note. Middle row: Heat transport (PW). Lower row: Total volume transport (Sv) and split into density classes; numbers in brackets denote the percentage of the total transport.

diminishing northward salt transport by the IC that reaches its minimum in 2017–2018. From 2018 to 2019 onwards, the northward salt transport recovers but remains lower than at the start of the record.

The IC heat transport shows a different evolution than freshwater transport (red line in Figures 7a, Table 1). Clearly, the correlation between heat and freshwater transport changes throughout the observed time period (Figure 7a). We find a strong anti-correlation between heat and freshwater transport before the arrival of the salinity anomaly until 2016 ($r = -0.79$, all correlations are significant at the 95% confidence interval), after which the correlation decreases to $r = -0.22$. This change in the correlation is related to the changes in the freshwater transport in response to the salinity anomaly rather than to changes in the heat transport. Throughout the 8 years, the heat transport increases associated with the increasing velocities and the slight warming of the waters in the upper east of the array.

To investigate the relative importance of salinity versus velocity changes in the freshwater transport in a simplified way, we compute the freshwater transport from both the varying velocity and salinity field (Equation 3) with the other parameter kept at the 8-year mean. In varS, the salinity is varying as observed and the velocities are assumed constant at this long-term mean value. In varV, the salinity is kept constant, and the velocity is varying as observed. Figure 7b shows both the time series constructed this way and the actual total freshwater transport. The varS-time series (orange) resembles the actual freshwater transport on annual time scales or longer, resulting in a moderate correlation to the total freshwater transport ($r = 0.53$). The velocity field is responsible for variability on shorter time scales resulting in a similar moderate correlation ($r = 0.59$). Overall, the freshwater transport is driven both by variations in the salinity and velocity field.

The influence of the velocity and salinity fields on the freshwater transport can vary over the water column. To assess the variability of freshwater transport more closely, we divide the freshwater transport up into waters of three density classes: the upper water column (Layer 1: $\sigma_0 \leq 27.55$ kg m^3), the intermediate waters (Layer 2: $27.55 < \sigma_0 < 27.8$ kg m^3), and the deep overflow layer (Layer 3: $\sigma_0 \geq 27.8$ kg m^3; these isopycnals are marked in Figures 2 and 3).

We show the respective effects of salinity and velocity on freshwater transport for each layer in Figure S1 of Supporting Information S1. The waters above the $\sigma_0 = 27.55$ kg m^{-3}—isopycnal (Layer 1, Figure S1a in Supporting Information S1) strongly correlate with the freshwater transport computed by a variable salinity field ($r = 0.6$). The correlation to the varying velocity field is slightly weaker ($r = 0.54$). Changes in the freshwater transport in the upper most layer are therefore can therefore be equally related to changes in velocity or salinity. The waters between 27.55 and 27.8 kg m^{-3} (Layer 2, Figure S1b in Supporting Information S1) still show a moderate correlation ($r = 0.47$) with a varying salinity field, but the effect of changing velocity field dominates ($r = 0.69$). The freshwater transport of the lowermost layers is mainly driven by the velocity field (Layer 3, Figure S1c in Supporting Information S1, $r = 0.91$), but still experience a moderate influence from the salinity field ($r = 0.5$). At depth, the overall trend is driven by variations in salinity, but variability in shorter time scales is

driven by variations in velocity. The relationship between salinity and freshwater transport is strongest in the uppermost layer that experienced strongest freshening. As the impact of the salinity anomaly decreases over depth, the influence of the velocity field on the freshwater transport increases.

To investigate the contribution of each layer to the total freshwater transport and possible changes therein, we show the respective freshwater transport time series per layer (Figure 7c). Before the arrival of the salinity anomaly (2014/2015), the upper (cyan line) and intermediate layer (light blue line) both equally contribute to the total freshwater transport (−6.4, −7.3 mSv). Between 2016 and 2018, at the peak of the salinity anomaly, the contribution drastically changes. In 2017–2018, the upper layer reveals a positive northward freshwater transport (+0.3 mSv). The freshwater transport in the intermediate layer changes to −3.0 mSv. After slightly recovering form the first drop in salinity the freshwater transport experiences a second drop in 2021/2022. As most changes happen in the upper layer, the correlation of its freshwater transport to the total is strongest. Even though the deepest layer was least affected by the salinity anomaly, we find a long-term trend of decreasing northward salt transport (−1.4 mSv in 14/15 to −0.4 mSv in 21/22).

Next, we correlate each layer of volume transport with its corresponding layer of freshwater transport to investigate possible impacts on volume transport (Figures 7c and 7d). The lower the correlation, the stronger changes in freshwater transport can be related to changes in salinity rather than changes in the volume transport. The freshwater transport of the upper layer, that experienced strongest changes in salinity, is weakly anti-correlated to its corresponding layer of volume transport ($r = -0.12$). This again highlights that the changes in freshwater transport are attributable to variations in salinity, not in velocity. In contrast, the freshwater transport in the intermediate layer is weakly but significantly anticorrelated to the intermediate layer volume transport ($r = -0.35$). As shown in Figure S1 of Supporting Information S1, this layer does experience a stronger contribution from the varying velocity field. The negative correlation arises from the fact that an increase in volume transport leads to an increase in the northward salt transport of the saline IC and hence to a decrease in freshwater transport.

To highlight the major salinity changes in the upper layers, we now investigate the respective contribution of each layer of volume transport to the total transport. The total volume transport increases from 8.3 Sv in 2014/2015 to 11.7 Sv in 2021/2022 with strong year-to-year variability (Table 1). The overall increase in transport agrees with the increase in the sea surface height (SSH) gradient between the SSH minimum in the Irminger Sea and the top of the Reykjanes Ridge (Figure S2 in Supporting Information S1). The gradient increased from by 4 cm between 14/16 and 20/22. Fried and de Jong (2022) already showed that on interannual time scales the basin-wide density gradient controls the transport variability of the IC.

In 14/15, the upper layer only contributes with 1.7 Sv to the total transport, the intermediate layer with 5.0 Sv. During the anomaly, the upper and intermediate layers nearly equally contribute to the total transport (3.3 and 3.5 Sv in 2017–2018). The contribution of the upper layer stays high until the end of the record with 4.2 Sv. The contribution of the deepest layer decreases in response to the freshening (1.6 Sv in 14/15 to 0.7 Sv in 21/22).

In summary, the decrease in northward salt transport (increase in freshwater transport) changed the volume transport composition of the IC to a larger contribution of lighter waters.

6. Discussion and Conclusion

In this study, we investigated the imprint of the recent salinity anomaly described by Holliday et al. (2020) on salinity changes over the whole water column of the IC using high-resolution mooring data from 2014 to 2022. To put our results into perspective with variations on basin-wide spatial scales and on longer timescales, we combined this with hydrographic sections across the Irminger Sea and the Iceland Basin since 1,990.

At the IC array, the freshwater anomaly decreased the salinity over the entire upper 1,500 m of the water column. Therefore, this anomaly should no longer be seen as a near surface anomaly. This represents a decreasing northward salt transport, as it indicates the IC's salinity gets closer to the used reference salinity (34.92 PSU). Based on our analyses, we attribute the changes in freshwater transport in the upper layer to the salinity changes, rather than to volume transport changes.

Previous studies showed that the salinity anomaly reached the Irminger Sea from the Iceland Basin (Biló et al., 2022; Devana et al., 2021). There, low salinity waters arrived in the eastern Iceland Basin in autumn 2015

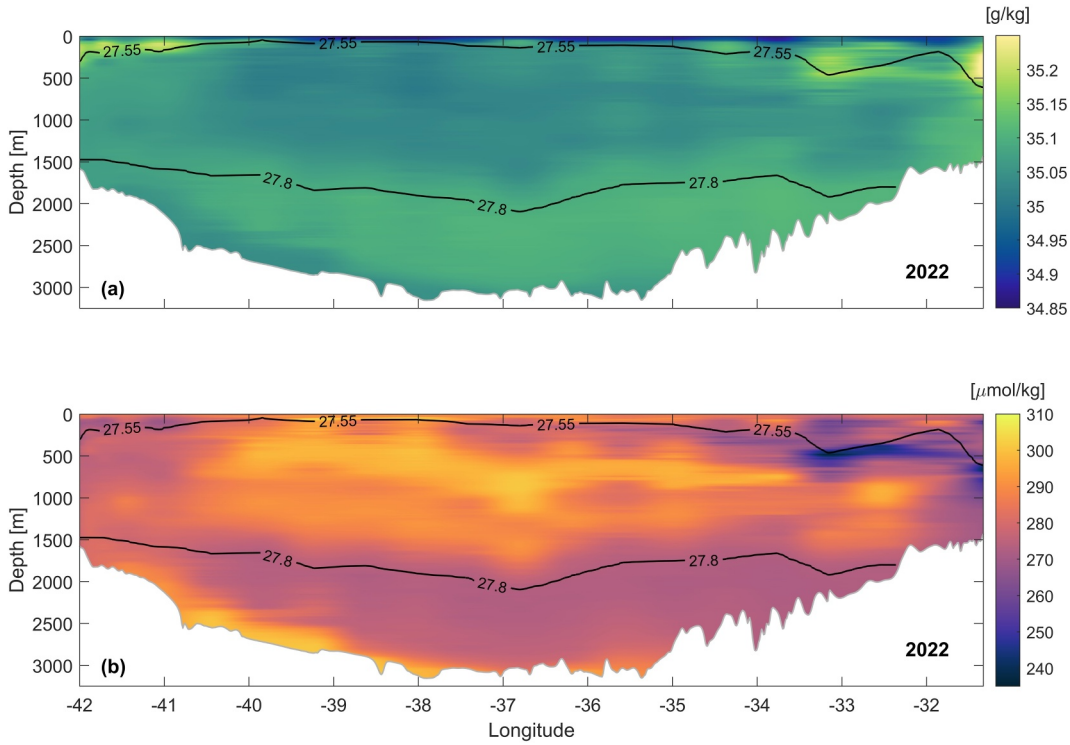

Figure 8. Salinity and Oxygen Section at OSNAP East for the Irminger Sea from 2022. (a) Salinity across the Irminger Sea from a hydrographic ship section in summer 2022 (shading) overlaid with isopycnals; (b) same as (a) but for oxygen.

(Devana et al., 2021). The anomaly reached the eastern flank of the Reykjanes Ridge by summer 2016 which agrees with our results at the IC array (Figure 2). This suggests a strong and fast connection of the upper layers across the Reykjanes Ridge. This is corroborated by assessing the lead-lag correlation between the mean salinity anomaly at 300–500 m for the moorings on its eastern and western flanks (IC4 and M1), which peaks at lag zero ($r = 0.78$).

Further investigation of the recent salinity anomaly using hydrographic sections showed that the salinity anomaly extended across the Irminger Sea. By summer 2022, oxygen measurements along OSNAP East reveal that waters with the same oxygen levels and low in salinity spread out from the central Irminger Sea (Figure 8). The increase of oxygen through deep convection in the Irminger Sea has been shown by Fröb et al. (2016) using observational data with a focus on the strong convection of the winter 2014/2015.

Even though deep convection in the central Irminger Sea was partially damped by the freshwater anomaly in the 2018/2019 and the 2019/2020 winters (Bilo et al., 2022), it returned in the following years and mixed down the slightly diluted freshwater anomaly into deeper layers. Those high oxygen waters in 2022 were then brought toward the IC, which could likely explain the delayed and diluted freshening signal in the deeper part of the water column compared to the surface freshening.

Additionally, the freshening at depth could be advected from the Iceland Basin to the Irminger Sea through Bight Fracture Zone. Multiple studies investigated the mixing of the salinity anomaly into the ISOW in the Iceland Basin (Devana et al. (2021); Chafik and Holliday (2022)). Devana et al. (2021) state that the salinity changes in the overflow plume are directly related to changes in the upper ocean through entrainment. Deep waters that freshened in the Iceland Basin through this mechanism would arrive at the IC array much later than surface waters. Similarly, Desbruyeres et al. (2022) studied the entrainment of freshening signals into the Denmark Strait Overflow Water (DSOW) that were likely responsible for a warming-to-cooling reversal of the deep water masses in the Irminger Sea.

Using a combination of hydrographic ocean analysis and mooring data, Biló et al. (2022) show that the surface anomaly freshened the upper Irminger Sea waters to values as fresh as in the early 1990s. Our results showed

that indeed water across the whole basin reached salinities as low as in the 1990s. At the IC array, waters below 500 m were even fresher in 2022 than in 1992. We conclude that the IC is in its freshest state observed since the 1990s.

In Fried and de Jong (2022), we showed that the basin-wide density gradient influences the transport variability at the IC array. We used 28 years of monthly reanalysis data to show that the increased volume transport during the 1990s was driven by a strong density gradient between the central Irminger Sea and the top of the Reykjanes Ridge. When the gradient was weak instead, around 2010/2011, the IC reached its lowest volume transport. We concluded that changes in the density gradient across the Irminger Sea can impact the IC volume transport. So, the gradient between the central Irminger Sea and the top of the Reykjanes Ridge must be carefully considered when interpreting changes in the transport variability of IC. Especially as the salinity anomaly peaked at different times along the OSNAP East line.

Our results on the IC transport are sensitive to whether the mooring array captures the entire northward flow of the IC. Especially its western core is very variable in location. A weak transport event can therefore also be caused by the western core not being fully captured by the westernmost mooring. Results presented here hence consider the IC transport as the transport within the boundaries of the mooring array. In addition to the spatial variations of the western core, Fried and de Jong (2022) showed that the transport can also be influenced by mesoscale variability within the mooring array. Basin-wide observations in the Irminger Sea therefore remain crucial to understand and disentangle the mechanisms driving the transport variability of the IC.

Here, we found that the volume transport of lighter waters ($\sigma < 27.55$ kg m^{-3}) strongly increased due to the freshening of the surface waters. In 2014–2015, the waters lighter than 27.55 kg m^{-3} contributed with 1.7 Sv to the total transport. By 2021–2022, this increased to 4.2 Sv. The transport of intermediate waters was comparable at the beginning and at the end of the record. The overall increase in volume transport is likely a combination of the increased transport in the upper layers and the changing velocity structure of the IC. Specifically, the location of the IC's western core moved further east throughout the observed time period.

In this study, we showed that the warm and saline IC drastically freshened in response to the most recent salinity anomaly, resulting in an increase in the northward transport of lighter and fresher waters. If this water further enters the convection regions in the subpolar gyre, it has the potential to suppress convection. However, once these freshwater anomalies are distributed over a large part of the water column the impact on stratification decreases. Still, a changed northward IC transport by density class may impact the characteristics of the overturning in the Northeastern Atlantic, in particular its strength and the density at which it peaks.

In the North Atlantic, this most recent freshwater anomaly, that was first described by Holliday et al. (2020), developed in the Labrador Sea from anomalous wind patterns that diverted freshwater from the Labrador Current in 2012. From there, it propagated eastward as a surface anomaly with the circulation of the subpolar gyre and arrived in the western Iceland Basin by 2015. There, it got partly entrained in the ISOW layer (Devana et al., 2021). By summer 2016, it entered the Irminger Sea (Bilo et al., 2022; de Jong et al., 2020) where it contributed to suppressing deep convection. Since then, the anomaly was mixed down into the water column and has freshened the Irminger Sea to a large spatial extent as shown in this study. Notably, this anomaly also entered the Nordic Seas from the Iceland Basin (Asbjørnsen et al., 2021; Mork et al., 2014, 2019) and likely freshened the DSOW layer via entrainment (Desbruyeres et al., 2021, 2022) affecting its transport in the subpolar gyre (Koman et al., 2024). Following the cyclonic circulation of the subpolar gyre, the diluted freshwater anomaly returned to the Labrador Sea, where it potentially added to the most recent larger freshwater influx from the Arctic, causing the shutdown of convection in 2023 (Yashayaev, 2024) and potentially affecting all main pathways of the subpolar overturning. Finally, the impacts of strong freshwater anomalies in the Subpolar North Atlantic go beyond impacts on the oceanic overturning and gyre circulations. Freshwater events can cause cold anomalies that in turn affect surface heat-flux patterns and, consequently, the low-frequency climate variability and large-scale weather patterns over western Europe (Oltmanns et al., 2020, 2024).

Data Availability Statement

We used mooring data from 2014 to 2022 from five deployments that are publicly available per deployment under: M.F. de Jong and de Steur, L, (2016). High-resolution current meter and hydrographic data from the

Irminger Current mooring array 2014–2015. NIOZ Royal Netherlands Institute for Sea Research. Data set. https://doi.org/10.4121/uuid:77b2c4fc-c253-4494-91bd-8d1ef66a014a M.F. de Jong and de Steur, L., (2019). High-resolution current meter and hydrographic data from the Irminger Current mooring array 2015–2016. NIOZ Royal Institute for Sea Research. Data set. https://doi.org/10.4121/uuid:9ae97ceb-39e4-43ec-abdb-614103285c16 de Jong, M. F., and N. Fried (2021a). "High-resolution current meter and hydrographic data from the Irminger Current mooring array 2016 to 2018", https://doi.org/10.25850/nioz/7b.b.nb de Jong, M. F., and N. Fried (2021b). "High-resolution current meter and hydrographic data from the Irminger Current mooring array 2018 to 2020", https://doi.org/10.25850/nioz/7b.b.pb de Jong, M. F., and N. Fried (2024). "High-resolution current meter and hydrographic data from the Irminger Current mooring array 2020 to 2022", https://doi.org/10.25850/nioz/7b.b.af. In this study we used the gridded field for the entire time period 2014–2022 that has been published under: Fried, N. (2024). "Gridded high-resolution current meter and hydrographic data from the Irminger Current mooring array from 2014 to 2022", https://doi.org/10.25850/nioz/7b.b.0f. In addition, we used hydrographic sections from 1990 to 2022. From 1990 to 2004 the near-annual surveys of the AR7 hydrographic section can be downloaded via http://cchdo.ucsd.edu/. The OVIDE sections from 2002, 2004, 2006, 2008 and 2010 are available under: Daniault Nathalie, Mercier Herle, Lherminier Pascale (2016). Gridded property and transport data of the biennial Greenland-Portugal A25 OVIDE line. SEANOE. https://doi.org/10.17882/46446. The section data from 2014 to 2022 made freely available by the OSNAP (Overturning in the Subpolar North Atlantic Program) project and all the national programs that contribute to it (www.o-snap.org). The 2015 OSNAP section data are available at https://www.seanoe.org/data/00481/59302/ (de Jong & de Steur, 2019). The 2020 OSNAP data are available https://dataverse.nioz.nl/dataset.xhtml?persistentId=doi:10.25850/nioz/7b.b.1f (de Jong, 2023). The 2022 OSNAP section data are available at https://cchdo.ucsd.edu/cruise/33VB20220819 (Straneo, 2023). The calibrated oxygen data from this section is published as: Fogaren, K. E., Palevsky, H. I. (2024) Bottle-calibrated dissolved oxygen (DO) profiles from US Overturning in the Subpolar North Atlantic Program (OSNAP) cruises in 2020 and 2022 (AR45 and AR69-03). Biological and Chemical Oceanography Data Management Office (BCO-DMO). http://lod.bco-dmo.org/id/dataset/933743.

Acknowledgments

We thank all scientists and mariners involved in the OSNAP project who went to sea to collect the observational data used in this study. This project was funded by the European Union seventh Framework Program (FP7 2007–2013) under Grant 308299 (NACLIM), Horizon 2020 Research and Innovation Program under Grant 727852 (Blue-Action), the Innovational Research Incentives Scheme of the Netherlands Organization for Scientific Research (NWO) under Grant 016. Vidi.189.130, and the Royal Netherlands Institute for Sea Research. T. C. B. acknowledges the funding from the National Science Foundation under grant OCE1948198 and the NOAA's Global Ocean Monitoring and Observing program (FundRef number 100007298); NOAA's Climate Program Office, Climate Observations and Monitoring, and Climate Variability and Predictability programs under NOFO NOAA-OAR-CPO–2021–2006389 with additional NOAA Atlantic Oceanographic and Meteorological Laboratory support. Support for oxygen analysis for the 2022 section was provided by the U.S. National Science Foundation (OCE-1947970 to H. I. P.). This research was carried out in part under the auspices of the Cooperative Institute for Marine and Atmospheric Studies, a cooperative institute of the University of Miami and the National Oceanic and Atmospheric Administration (NOAA), cooperative agreement NA 20OAR4320472.

References

Asbjørnsen, H., Johnson, H. L., & Årthun, M. (2021). Variable nordic seas inflow linked to shifts in North Atlantic circulation. *Journal of Climate*, *34*(17), 7057–7071.

Belkin, I. M. (2004). Propagation of the "great salinity anomaly" of the 1990s around the northern North Atlantic. *Geophysical Research Letters*, *31*(8). https://doi.org/10.1029/2003gl019334

Belkin, I. M., Levitus, S., Antonov, J., & Malmberg, S. A. (1998). "Great salinity anomalies" in the North Atlantic. *Progress in Oceanography*, *41*(1), 1–68. https://doi.org/10.1016/s0079-6611(98)00015-9

Biló, T. C., Straneo, F., Holte, J., & Le Bras, I. A. (2022). Arrival of New great salinity anomaly weakens convection in the Irminger Sea. *Geophysical Research Letters*, *49*(11), e2022GL098857. https://doi.org/10.1029/2022gl098857

Chafik, L., & Holliday, N. P. (2022). Rapid communication of upper-ocean salinity anomaly to deep waters of the Iceland Basin indicates an AMOC short-cut. *Geophysical Research Letters*, *49*(3), e2021GL097570. https://doi.org/10.1029/2021gl097570

Chafik, L., Rossby, T., & Schrum, C. (2014). On the spatial structure and temporal variability of poleward transport between Scotland and Greenland. *Journal of Geophysical Research: Oceans*, *119*(2), 824–841. https://doi.org/10.1002/2013jc009287

Daniault Nathalie, Mercier Herle, Lherminier Pascale. (2016). Gridded property and transport data of the biennial Greenland-Portugal A25 OVIDE line. *SEANOE*. https://doi.org/10.17882/46446

de Jong, F. (2023). Calibrated CTD data from OSNAP Pelagia cruise 64PE473 in July–Aug 2020. https://dataverse.nioz.nl/dataset.xhtml?persistentId=doi:10.25850/nioz/7b.b.1f

de Jong, M., & de Steur, L. (2019). *Cruise 64PE400: Hydrographic survey of the Irminger Sea in July 2015 for the overturning in the Subpolar North Atlantic Program (OSNAP)*. SEANOE. https://doi.org/10.17882/59302

de Jong, M. F., & de Steur, L. (2016). Strong winter cooling over the Irminger Sea in winter 2014–2015, exceptional deep convection, and the emergence of anomalously low SST. *Geophysical Research Letters*, *43*(13), 7106–7113. https://doi.org/10.1002/2016gl069596

de Jong, M. F., de Steur, L., Fried, N., Bol, R., & Kritsotalakis, S. (2020). Year-round measurements of the Irminger Current: Variability of a two-core current system observed in 2014–2016. *Journal of Geophysical Research: Oceans*, *125*(10), e2020JC016193. https://doi.org/10.1029/2020jc016193

de Jong, M. F., Fogaren, K. E., Le Bras, I. A. A., McRaven, L. T., & Palevsky, H. I. (2023). *Convection in the central Irminger Sea; insights into variability and the roles of surface forcing and stratification from 19 years of high resolution mooring data*. Authorea Preprints.

de Jong, M. F., & Fried, N. (2021a). High-resolution current meter and hydrographic data from the Irminger current mooring array 2016–2018 [Dataset]. NIOZ, V1. https://doi.org/10.25850/nioz/7b.b.nb

de Jong, M. F., & Fried, N. (2021b). High-resolution current meter and hydrographic data from the Irminger current mooring array 2018–2020 [Dataset]. NIOZ, V10. https://doi.org/10.25850/nioz/7b.b.pb

de Jong, M. F., & Fried, N. (2024). High-resolution current meter and hydrographic data from the Irminger current mooring array 2020–2022 [Dataset]. NIOZ, V1. https://doi.org/10.25850/nioz/7b.b.af

de Jong, M. F., Oltmanns, M., Karstensen, J., & de Steur, L. (2018). Deep convection in the Irminger Sea observed with a dense mooring array. *Oceanography*, *31*(1), 50–59. https://doi.org/10.5670/oceanog.2018.109

de Jong, M. F., van Aken, H. M., Våge, K., & Pickart, R. S. (2012). Convective mixing in the central Irminger Sea: 2002–2010. *Deep Sea Research Part I: Oceanographic Research Papers*, *63*, 36–51. https://doi.org/10.1016/j.dsr.2012.01.003

Desbruyères, D., Chafik, L., & Maze, G. (2021). A shift in the ocean circulation has warmed the subpolar North Atlantic Ocean since 2016. *Communications Earth & Environment*, *2*(1), 48. https://doi.org/10.1038/s43247-021-00120-y

Desbruyères, D. G., Bravo, E. P., Thierry, V., Mercier, H., Lherminier, P., Cabanes, C., et al. (2022). Warming-to-Cooling reversal of overflow-derived water masses in the Irminger Sea during 2002–2021. *Geophysical Research Letters*, *49*(10), e2022GL098057. https://doi.org/10.1029/2022gl098057

Devana, M. S., Johns, W. E., Houk, A., & Zou, S. (2021). Rapid freshening of Iceland Scotland overflow water driven by entrainment of a major upper ocean salinity anomaly. *Geophysical Research Letters*, *48*(22), e2021GL094396. https://doi.org/10.1029/2021gl094396

Dickson, R. R., Meincke, J., Malmberg, S. A., & Lee, A. J. (1988). The "great salinity anomaly" in the northern North Atlantic 1968–1982. *Progress in Oceanography*, *20*(2), 103–151. https://doi.org/10.1016/0079-6611(88)90049-3

Eldevik, T., Straneo, F., Sandø, A. B., & Furevik, T. (2005). Pathways and export of Greenland Sea Water. In *The nordic seas: An integrated perspective*.

Fogaren, K. E., & Palevsky, H. I. (2024). Bottle-calibrated Dissolved Oxygen (DO) profiles from US overturning in the Subpolar North Atlantic Program (OSNAP) cruises in 2020 and 2022 (AR45 and AR69-03). *Biological and Chemical Oceanography Data Management Office (BCO-DMO). (Version 1)*. https://doi.org/10.26008/1912/bco-dmo.933743

Fox-Kemper, B., Hewitt, H. T., Xiao, C., Aðalgeirsdóttir, G., Drijfhout, S. S., Edwards, T. L., & Yu, Y. (2021). Ocean, cryosphere, and sea level change. In *Climate change 2021: The physical science basis. Contribution of working group I to the sixth assessment report of the intergovernmental panel on climate change* (pp. 1211–1361). Cambridge University Press.

Fried, N. (2024). Gridded high-resolution current meter and hydrographic data from the Irminger Current mooring array from 2014–2022 [Dataset]. NIOZ, V1. https://doi.org/10.25850/nioz/7b.b.0f

Fried, N., & de Jong, M. F. (2022). The role of the Irminger Current in the Irminger Sea northward transport variability. *Journal of Geophysical Research: Oceans*, *127*(3), e2021JC018188. https://doi.org/10.1029/2021jc018188

Fried, N., Katsman, C. A., & de Jong, M. F. (2024). Where do the two cores of the Irminger current come from? A Lagrangian study using a 1/10° ocean model simulation. *Journal of Geophysical Research: Oceans*, *129*, e2023JC020713. https://doi.org/10.1029/2023JC020713

Fröb, F., Olsen, A., Våge, K., Moore, G. W. K., Yashayaev, I., Jeansson, E., & Rajasakaren, B. (2016). Irminger Sea deep convection injects oxygen and anthropogenic carbon to the ocean interior. *Nature Communications*, *7*(1), 13244. https://doi.org/10.1038/ncomms13244

Fu, Y., Lozier, M. S., Biló, T. C., Bower, A. S., Cunningham, S. A., Cyr, F., et al. (2023). Seasonality of the meridional overturning circulation in the subpolar North Atlantic. *Communications earth & environment*, *4*(1), 181. https://doi.org/10.1038/s43247-023-00848-9

Gelderloos, R., Straneo, F., & Katsman, C. A. (2012). Mechanisms behind the temporary shutdown of deep convection in the Labrador Sea: Lessons from the great salinity anomaly years 1968–71. *Journal of Climate*, *25*(19), 6743–6755. https://doi.org/10.1175/jcli-d-11-00549.1

Holliday, N. P., Bersch, M., Berx, B., Chafik, L., Cunningham, S., Florindo-López, C., et al. (2020). Ocean circulation causes the largest freshening event for 120 years in eastern subpolar North Atlantic. *Nature Communications*, *11*(1), 585. https://doi.org/10.1038/s41467-020-14474-y

Holliday, N. P., Hughes, S. L., Bacon, S., Beszczynska-Möller, A., Hansen, B., Lavin, A., et al. (2008). Reversal of the 1960s to 1990s freshening trend in the northeast North Atlantic and Nordic seas. *Geophysical Research Letters*, *35*(3). https://doi.org/10.1029/2007gl032675

Jackson, L. C., Alastrué de Asenjo, E., Bellomo, K., Danabasoglu, G., Haak, H., Hu, A., & Swingedouw, D. (2022). Understanding AMOC stability: The North Atlantic hosing model intercomparison project. *Geoscientific Model Development Discussions*, *2022*, 1–32.

Jackson, L. C., & Wood, R. A. (2018). Timescales of AMOC decline in response to fresh water forcing. *Climate Dynamics*, *51*(4), 1333–1350. https://doi.org/10.1007/s00382-017-3957-6

Kim, W. M., Yeager, S., & Danabasoglu, G. (2021). Revisiting the causal connection between the great salinity anomaly of the 1970s and the shutdown of Labrador Sea deep convection. *Journal of Climate*, *34*(2), 675–696. https://doi.org/10.1175/jcli-d-20-0327.1

Knutsen, Ø., Svendsen, H., Østerhus, S., Rossby, T., & Hansen, B. (2005). Direct measurements of the mean flow and eddy kinetic energy structure of the upper ocean circulation in the NE Atlantic. *Geophysical Research Letters*, *32*(14), L14604. https://doi.org/10.1029/2005GL023615

Koman, G., Bower, A. S., Holliday, N. P., Furey, H. H., Fu, Y., & Biló, T. C. (2024). Observed decrease in deep western boundary current transport in subpolar North Atlantic. *Nature Geoscience*, *17*(11), 1–6. https://doi.org/10.1038/s41561-024-01555-6

Koman, G., Johns, W. E., & Houk, A. (2020). Transport and evolution of the East Reykjanes Ridge Current. *Journal of Geophysical Research: Oceans*, *125*(10), e2020JC016377. https://doi.org/10.1029/2020jc016377

Lazier, J., Pickart, R., & Rhines, P. (2001). Deep convection. *International Geophysics*, *77*, 387–400.

Lazier, J. R. (1973). The renewal of Labrador Sea water. In *Deep Sea research and oceanographic abstracts*, (Vol. 20(4), pp. 341–353). Elsevier. https://doi.org/10.1016/0011-7471(73)90058-2

Lazier, J. R. (1980). Oceanographic conditions at ocean weather ship Bravo, 1964–1974. *Atmosphere-Ocean*, *18*(3), 227–238. https://doi.org/10.1080/07055900.1980.9649089

Lherminier, P., Mercier, H., Gourcuff, C., Alvarez, M., Bacon, S., & Kermabon, C. (2007). Transports across the 2002 Greenland-Portugal Ovide section and comparison with 1997. *Journal of Geophysical Research*, *112*(C7). https://doi.org/10.1029/2006jc003716

Li, F., Lozier, M. S., Bacon, S., Bower, A. S., Cunningham, S. A., De Jong, M. F., et al. (2021). Subpolar North Atlantic western boundary density anomalies and the meridional overturning circulation. *Nature Communications*, *12*(1), 3002. https://doi.org/10.1038/s41467-021-23350-2

Lozier, M. S., Bacon, S., Bower, A. S., Cunningham, S. A., de Jong, F. M., de Steur, L., et al. (2017). Overturning in the Subpolar North Atlantic program: A new international ocean observing system. *Bulletin of the American Meteorological Society*, *98*(4), 737–752. https://doi.org/10.1175/BAMS-D-16-0057.1

Lozier, M. S., Li, F., Bacon, S., Bahr, F., Bower, A. S., Cunningham, S. A., et al. (2019). A sea change in our view of overturning in the subpolar North Atlantic. *Science*, *363*(6426), 516–521. https://doi.org/10.1126/science.aau6592

Marshall, J., & Schott, F. (1999). Open-ocean convection: Observations, theory, and models. *Reviews of Geophysics*, *37*(1), 1–64. https://doi.org/10.1029/98rg02739

McDougall, T. J., & Barker, P. M. (2011). Getting started with TEOS-10 and the Gibbs Seawater (GSW) oceanographic toolbox. *Scor/Iapso WG*, *127*(532), 1–28.

Mercier, H., Lherminier, P., Sarafanov, A., Gaillard, F., Daniault, N., Desbruyères, D., et al. (2015). Variability of the meridional overturning circulation at the Greenland–Portugal OVIDE section from 1993 to 2010. *Progress in Oceanography*, *132*, 250–261. https://doi.org/10.1016/j.pocean.2013.11.001

Messias, M. J., Watson, A. J., Johannessen, T., Oliver, K. I. C., Olsson, K. A., Fogelqvist, E., et al. (2008). The Greenland Sea tracer experiment 1996–2002: Horizontal mixing and transport of Greenland Sea intermediate water. *Progress in Oceanography*, *78*(1), 85–105. https://doi.org/10.1016/j.pocean.2007.06.005

Mork, K. A., Skagseth, Ø., Ivshin, V., Ozhigin, V., Hughes, S. L., & Valdimarsson, H. (2014). Advective and atmospheric forced changes in heat and fresh water content in the Norwegian Sea, 1951–2010. *Geophysical Research Letters*, *41*(17), 6221–6228. https://doi.org/10.1002/2014gl061038

Mork, K. A., Skagseth, Ø., & Søiland, H. (2019). Recent warming and freshening of the Norwegian Sea observed by Argo data. *Journal of Climate*, *32*(12), 3695–3705. https://doi.org/10.1175/jcli-d-18-0591.1

Oltmanns, M., Holliday, N. P., Screen, J., Moat, B. I., Josey, S. A., Evans, D. G., & Bacon, S. (2024). European summer weather linked to North Atlantic freshwater anomalies in preceding years. *Weather Clim. Dynam.*, *5*(1), 109–132. https://doi.org/10.5194/wcd-5-109-2024

Oltmanns, M., Karstensen, J., Moore, G. W. K., & Josey, S. A. (2020). Rapid cooling and increased storminess triggered by freshwater in the North Atlantic. *Geophysical Research Letters*, *47*(14), e2020GL087207. https://doi.org/10.1029/2020gl087207

Petit, T., Mercier, H., & Thierry, V. (2019). New insight into the formation and evolution of the East Reykjanes Ridge Current and Irminger current. *Journal of Geophysical Research: Oceans*, *124*(12), 9171–9189. https://doi.org/10.1029/2019jc015546

Pickart, R. S., & Spall, M. A. (2007). Impact of Labrador Sea convection on the North Atlantic meridional overturning circulation. *Journal of Physical Oceanography*, *37*(9), 2207–2227. https://doi.org/10.1175/jpo3178.1

Pickart, R. S., Spall, M. A., Ribergaard, M. H., Moore, G. K., & Milliff, R. F. (2003). Deep convection in the Irminger Sea forced by the Greenland tip jet. *Nature*, *424*(6945), 152–156. https://doi.org/10.1038/nature01729

Piron, A., Thierry, V., Mercier, H., & Caniaux, G. (2016). Argo float observations of basin-scale deep convection in the Irminger sea during winter 2011–2012. *Deep Sea Research Part I: Oceanographic Research Papers*, *109*, 76–90. https://doi.org/10.1016/j.dsr.2015.12.012

Sarafanov, A., Falina, A., Mercier, H., Sokov, A., Lherminier, P., Gourcuff, C., et al. (2012). Mean full-depth summer circulation and transports at the northern periphery of the Atlantic Ocean in the 2000s. *Journal of Geophysical Research*, *117*(C1). https://doi.org/10.1029/2011jc007572

Sterl, M. F., & de Jong, M. F. (2022). Restratification structure and processes in the Irminger Sea. *Journal of Geophysical Research: Oceans*, *127*(12), e2022JC019126. https://doi.org/10.1029/2022jc019126

Stouffer, R. J., Yin, J., Gregory, J. M., Dixon, K. M., Spelman, M. J., Hurlin, W., et al. (2006). Investigating the causes of the response of the thermohaline circulation to past and future climate changes. *J. Climate*, *19*, 1365–1387. https://doi.org/10.1175/JCLI3689.1

Straneo. (2023). CCHDO hydrographic data archive. In *CCHDO hydrographic data archive*. UC San Diego Library Digital Collections.

Thornalley, D. J., Oppo, D. W., Ortega, P., Robson, J. I., Brierley, C. M., Davis, R., et al. (2018). Anomalously weak Labrador Sea convection and Atlantic overturning during the past 150 years. *Nature*, *556*(7700), 227–230. https://doi.org/10.1038/s41586-018-0007-4

Våge, K., Moore, G. W. K., Jónsson, S., & Valdimarsson, H. (2015). Water mass transformation in the Iceland Sea. *Deep Sea Research Part I: Oceanographic Research Papers*, *101*, 98–109. https://doi.org/10.1016/j.dsr.2015.04.001

Våge, K., Pickart, R. S., Sarafanov, A., Knutsen, Ø., Mercier, H., Lherminier, P., et al. (2011). The Irminger Gyre: Circulation, convection, and interannual variability. *Deep Sea Research Part I: Oceanographic Research Papers*, *58*(5), 590–614. https://doi.org/10.1016/j.dsr.2011.03.001

van Aken, H. M., de Jong, M. F., & Yashayaev, I. (2011). Decadal and multi-decadal variability of Labrador Sea Water in the North-Western North Atlantic Ocean derived from tracer distributions: Heat budget, ventilation, and advection. *Deep Sea Research Part I: Oceanographic Research Papers*, *58*(5), 505–523. https://doi.org/10.1016/j.dsr.2011.02.008

Yashayaev, I. (2007). Hydrographic changes in the Labrador Sea, 1960–2005. *Progress in Oceanography*, *73*(3–4), 242–276. https://doi.org/10.1016/j.pocean.2007.04.015

Yashayaev, I. (2024). Intensification and shutdown of deep convection in the Labrador Sea were caused by changes in atmospheric and freshwater dynamics. *Communications Earth & Environment*, *5*(1), 156. https://doi.org/10.1038/s43247-024-01296-9

Yeager, S., & Danabasoglu, G. (2014). The origins of late-twentieth-century variations in the large-scale North Atlantic circulation. *Journal of Climate*, *27*(9), 3222–3247. https://doi.org/10.1175/jcli-d-13-00125.1

References From the Supporting Information

Schmidt, S., & Send, U. (2007). Origin and composition of seasonal Labrador Sea freshwater. *Journal of Physical Oceanography*, *37*(6), 1445–1454. https://doi.org/10.1175/JPO3065.1